IMMUNE NETWORK

Original Article

Check for updates

*Correspondence to
Sang-Il Lee
Department of Internal Medicine and Institute of Medical Science, Gyeongsang National University School of Medicine and Hospital, 79 Gangnam-ro, Jinju 52727, Korea.
Email: goldgu@gnu.ac.kr

[†]Hanna Lee, Ok-Yi Jeong, and Hee Jin Park contributed equally to this work.

ORCID iDs
Hanna Lee
https://orcid.org/0000-0002-2129-4269
Ok-Yi Jeong
https://orcid.org/0000-0001-9362-2746
Hee Jin Park
https://orcid.org/0000-0001-9415-9802
Sung-Lim Lee
https://orcid.org/0000-0002-1055-8097
Eun-yeong Bok
https://orcid.org/0000-0002-1045-9670

Promising Therapeutic Effects of Embryonic Stem Cells-Origin Mesenchymal Stem Cells in Experimental Pulmonary Fibrosis Models: Immunomodulatory and Anti-Apoptotic Mechanisms

Hanna Lee [1,2,†], Ok-Yi Jeong [2,†], Hee Jin Park [2,†], Sung-Lim Lee [3], Eun-yeong Bok [3], Mingyo Kim [2], Young Sun Suh [1,2], Yun-Hong Cheon [2], Hyun-Ok Kim [1,2], Suhee Kim [2], Sung Hak Chun [2], Jung Min Park [2], Young Jin Lee [4], Sang-Il Lee [2,*]

[1]Department of Internal Medicine, Gyeongsang National University Changwon Hospital, Changwon 51427, Korea
[2]Department of Internal Medicine and Institute of Medical Science, Gyeongsang National University School of Medicine and Hospital, Jinju 52727, Korea
[3]College of Veterinary Medicine and Research Institute of Life Sciences, Gyeongsang National University, Jinju 52828, Korea
[4]Cell Therapy Center, Daewoong Pharmaceutical, Co., Ltd., Yongin 17028, Korea

ABSTRACT

Interstitial lung disease (ILD) involves persistent inflammation and fibrosis, leading to respiratory failure and even death. Adult tissue-derived mesenchymal stem cells (MSCs) show potential in ILD therapeutics but obtaining an adequate quantity of cells for drug application is difficult. Daewoong Pharmaceutical's MSCs (DW-MSCs) derived from embryonic stem cells sustain a high proliferative capacity following long-term culture and expansion. The aim of this study was to investigate the therapeutic potential of DW-MSCs in experimental mouse models of ILD. DW-MSCs were expanded up to 12 passages for *in vivo* application in bleomycin-induced pulmonary fibrosis and collagen-induced connective tissue disease-ILD mouse models. We assessed lung inflammation and fibrosis, lung tissue immune cells, fibrosis-related gene/protein expression, apoptosis and mitochondrial function of alveolar epithelial cells, and mitochondrial transfer ability. Intravenous administration of DW-MSCs consistently improved lung fibrosis and reduced inflammatory and fibrotic markers expression in both models across various disease stages. The therapeutic effect of DW-MSCs was comparable to that following daily oral administration of nintedanib or pirfenidone. Mechanistically, DW-MSCs exhibited immunomodulatory effects by reducing the number of B cells during the early phase and increasing the ratio of Tregs to Th17 cells during the late phase of bleomycin-induced pulmonary fibrosis. Furthermore, DW-MSCs exhibited anti-apoptotic effects, increased cell viability, and improved mitochondrial respiration in alveolar epithelial cells by transferring their mitochondria to alveolar epithelial cells. Our findings indicate the strong potential of DW-MSCs in the treatment of ILD owing to their high efficacy and immunomodulatory and anti-apoptotic effects.

Keywords: Interstitial lung disease; Mesenchymal stem cell; Immunomodulation; Apoptosis; Mitochondria

Generated by xmlinkpress

IMMUNE NETWORK

Mingyo Kim
https://orcid.org/0000-0003-3744-8522
Young Sun Suh
https://orcid.org/0000-0002-5378-2590
Yun-Hong Cheon
https://orcid.org/0000-0002-0099-6253
Hyun-Ok Kim
https://orcid.org/0000-0002-0904-1584
Suhee Kim
https://orcid.org/0000-0002-9315-0360
Sung Hak Chun
https://orcid.org/0009-0007-3852-6066
Jung Min Park
https://orcid.org/0009-0006-5977-7801
Young Jin Lee
https://orcid.org/0000-0002-2325-5271
Sang-Il Lee
https://orcid.org/0000-0002-8283-7001

Abbreviations
Acta2, actin alpha 2, smooth muscle; AECIIs, type II alveolar epithelial cells; Bax, Bcl-2-associated X; Bcl-2, B-cell lymphoma-2; BLM, bleomycin; BPF, bleomycin-induced pulmonary fibrosis; CIA, collagen-induced arthritis; *Col1a1*, collagen type I alpha 1 chain; COVID-19, coronavirus disease-2019; COX-4, cytochrome c oxidase subunit 4; CTD-ILD, connective tissue disease-associated interstitial lung disease; *Ctgf*, connective tissue growth factor; DAB, 3,3′-diaminobenzidine; DW-MSCs, Daewoong Pharmaceutical's mesenchymal stromal cells; *Gapdh*, glyceraldehyde 3-phosphate dehydrogenase; hCOX-4, human nuclear-encoded subunit 4 of cytochrome c oxidase; *Il1*β, interluekin-1β; ILD, interstitial lung disease; IPF, idiopathic pulmonary fibrosis; MSC, mesenchymal stem cell; OCR, oxygen consumption rate; RA, rheumatoid arthritis; SMA, smooth muscle actin; SPC, surfactant protein C; *Tgfb1*, transforming growth factor-β; TNT, Tunneling nanotube; TUNEL, terminal deoxynucleotidyl transferase dUTP nick-end labeling; UIP, Usual interstitial pneumonia.

Author Contributions
Conceptualization: Lee H, Jeong OY, Park HJ, Lee SL, Lee SI; Data curation: Jeong OY, Park HJ, Bok EY, Kim M, Kim HO, Kim S, Chun SH, Park JM, Lee YJ; Formal analysis: Lee H, Jeong OY, Park HJ, Lee SL, Suh YS, Cheon YH, Kim HO, Kim S, Chun SH; Funding acquisition: Lee SI; Investigation: Park HJ, Lee

INTRODUCTION

Interstitial lung disease (ILD) is a serious condition characterized by inflammation and fibrosis of the lung interstitium, which can lead to respiratory failure and even death (1). ILD encompasses a diverse group of diseases, with idiopathic pulmonary fibrosis (IPF) and connective tissue disease-associated ILD (CTD-ILD) being the most common ILDs. IPF is the most common ILD of unknown etiology and is histopathologically characterized by usual interstitial pneumonia (UIP). This condition has a 50% probability of mortality within 2–3 years if left untreated (2,3). CTD-ILD has two main histopathological forms, UIP and non-specific interstitial pneumonia, which can occur in autoimmune conditions such as systemic sclerosis, rheumatoid arthritis (RA), polymyositis, and dermatomyositis (4). The UIP pattern generally has a poorer prognosis in patients with CTD-ILD (5). In patients with RA-ILD exhibiting UIP, the 5-year survival rate is as low as 36.6%, which is comparable to that of IPF (6,7). Consequently, intensive treatment is necessary for patients with IPF or CTD-ILD exhibiting UIP patterns.

ILD is characterized by repetitive and persistent damage to alveolar epithelial cells (AECs) and activation of immune cells and fibroblasts, resulting in excessive deposition of the extracellular matrix (8). Previously developed ILD therapies that aimed to reduce inflammation and immune activation, including those involving glucocorticoids and immunosuppressive agents, such as cyclophosphamide, azathioprine, and mycophenolate mofetil, have demonstrated limited efficacy (4,9). Recently, targeted agents used in CTD, such as IL-6 (e.g., tocilizumab), T-cell (e.g., abatacept), and B-cell (e.g., rituximab) inhibitors, have been investigated, but their effectiveness is also limited (10-13). Additionally, therapeutic agents that directly inhibit primary fibrotic pathways, such as pirfenidone and nintedanib, have shown some improvement in treatment outcomes; however, their effectiveness remains restricted (11,14). Furthermore, these agents are associated with frequent side effects that often lead many patients to reduce their dosage or discontinue use (15,16). Therefore, it is necessary to develop treatments for ILD with enhanced therapeutic effects and minimal side effects.

Preclinical studies have demonstrated the effectiveness of MSCs in treating ILD by effectively inhibiting the progression of fibrosis and reducing inflammation through various mechanisms (17-26). MSCs secrete paracrine factors that modulate immune cells and suppress inflammation and immune activation in alveoli (24). In addition, MSCs inhibit apoptosis and protect type II AECs (AECIIs), which play a role in the repair and regeneration of the lung tissue through the transfer of mitochondria (25-28). Additionally, the frequency of adverse events from MSCs was found to be relatively low in several phase 1 clinical trials for IPF patients and in a meta-analysis of patients with acute respiratory distress syndrome causing lung fibrosis (29-31). Collectively, these findings suggest that MSCs offer great potential as a therapeutic option for ILD, demonstrating minimal side effects and high efficacy.

Most preclinical animal experiments for ILD have used MSCs derived from adult tissues such as the bone marrow, adipose tissue, and umbilical cord (17-22). However, adult tissue-origin MSCs exhibit decreased paracrine capacity and proliferative ability with increasing age and passage number, thus posing a challenge in obtaining an adequate quantity and quality of these cells for commercial use in therapeutic applications (32-34). In contrast, embryonic-origin MSCs exhibit pluripotent stem cell-like characteristics, possess a higher expansion capacity, and have superior sustained paracrine abilities, thereby offering distinct advantages

SL, Suh YS, Cheon YH, Kim HO, Kim S, Lee SI;
Methodology: Lee H, Jeong OY, Park HJ, Lee
SL, Bok EY, Kim M, Suh YS, Cheon YH, Chun
SH, Park JM; Project administration: Lee SI;
Resources: Lee YJ, Lee SI; Supervision: Lee
SI; Validation: Lee H; Visualization: Jeong OY,
Park HJ, Bok EY; Writing - original draft: Lee
H, Jeong OY, Park HJ, Kim M, Lee YJ; Writing -
review & editing: Park HJ, Lee SI.

as cellular therapeutic agents in clinical settings (35,36). In a recent study on coronavirus disease-2019 (COVID-19), commercially produced Daewoong Pharmaceutical's mesenchymal stromal cells (DW-MSCs) derived from embryonic stem cells were used, revealing their potential as a cell therapy (37). However, further investigation is required to assess their efficacy in the treatment of ILD. Therefore, in the present study, we aimed to elucidate the mechanisms underlying the beneficial effects of DW-MSCs on ILD and provide insights into their therapeutic potential.

MATERIALS AND METHODS

DW-MSCs

Embryonic stem cell-derived mesenchymal stem cells (DW-MSCs, passage No. 12) were generously provided by Daewoong Pharmaceutical (Seoul, Korea). These cells originated from embryonic stem cells (SNUhES35) and were produced at a facility that follows the Good Manufacturing Practices. Following expansion and surface marker characterization, the cells were cryopreserved in liquid nitrogen after passage. DW-MSCs demonstrated the potential to differentiate into chondroblasts, osteoblasts, and adipocytes, and their quality was confirmed using various tests (37). Passage-12 DW-MSCs were used for in vivo experiments, whereas passage-13 and 14 DW-MSCs were used for *in vitro* experiments.

Animals

All animal experiments were conducted in accordance with the procedures approved by the Animal Experimentation Ethics Committee of Gyeongsang National University (GNU-200619-M0038). Male C57BL/6 mice, aged 8–10 wk, were purchased from Central Laboratory Animals (Seoul, Korea) and acclimated to specific pathogen-free conditions for at least 1 wk. All mice were housed in a room with a 12 h/12 h light/dark cycle, 50%±10% humidity, and a temperature of 22±3°C. The mice were provided with standard rodent chow and water *ad libitum*. The bleomycin-induced pulmonary fibrosis (BPF) mouse model was used as the animal model for IPF. Anesthesia was induced using avertin (500 mg/kg) and bleomycin (BLM; Dong-A ST, Seoul, Korea) was administered intratracheally (50 μl volume [1 U/kg] dissolved in PBS). DW-MSCs were injected into the tail veins of the mice at different doses and at various disease stages as follows:

(1) To determine the progression of pulmonary fibrosis, fibrosis was assessed histologically in the lung tissues of the mice at 4, 7, 14, and 21 days after BLM induction.

(2) To determine the optimal dose of DW-MSCs, a single injection of 1×10^5 or 1×10^6 DW-MSCs was administered on day 7 after BLM induction, and pulmonary fibrosis in the mice was evaluated on day 21.

(3) To determine the frequency of DW-MSC administration, single (on day 7) or serial (on days 7, 11, and 15) injections of 1×10^6 DW-MSCs were administered after BLM induction and the mice were sacrificed on day 21.

(4) To analyze the efficacy of DW-MSCs in early-phase BPF mice, 1×10^6 DW-MSCs were injected on day 4 after BLM induction and the mice were sacrificed on day 14.

(5) To analyze the efficacy of DW-MSCs in active-phase BPF mice, 1×10^6 DW-MSCs were injected on day 7 after BLM induction and the mice were sacrificed on day 21.

(6) To analyze the efficacy of DW-MSCs in the chronic persistent-phase BPF mice, 1×10^6 DW-MSCs were injected on day 21 after the first BLM induction (four doses of BLM, in total, were administered every other week) and the mice were sacrificed on day 56.

(7) To analyze the efficacy of nintedanib in BPF mice, 2×10^6 DW-MSCs were injected on day

4 after BLM induction and the mice were sacrificed on d21. Nintedanib (catalog No. S1010; Selleck Chemical, Houston, TX, USA) was orally administered at a dose of 25 mg/kg twice a day (50 mg/kg daily) starting the day after BLM induction.

(8) To analyze the efficacy of pirfenidone in BPF mice, 1×10^6 DW-MSCs were injected on day 7 after BLM induction and the mice were sacrificed on day 21. Pirfenidone was orally administered at a dose of 150 mg/kg/d 5 times a week for 2 wk after BLM induction (Pirespa Tab; Shiono Chemical, Osaka, Japan).

A collagen-induced arthritis (CIA) mouse model was also used as an animal model of RA. Seven male DBA/1J mice (9-wk-old) were purchased from Central Laboratory Animals. The primary immunization involved a mixture of bovine type II collagen (catalog No. 20022; Chondrex, Redmond, WA, USA) dissolved in 0.05 M acetic acid, at a concentration of 2 mg/ml, with complete Freund's Adjuvant (catalog No. F5881; Sigma-Aldrich Co., Toluca, Mexico) in a 1:1 ratio. Intradermal injections were administered at the base of the mouse tail. On day 21, booster injections of a mixture of bovine type II collagen and incomplete Freund's adjuvant (catalog No. 7002; Chondrex) were administered through intradermal tail injection. CIA mice were randomly divided into PBS- (CIA) and DW-MSC-treated (CIA/DW-MSC) groups. DW-MSCs (1×10^6) were administered as a single intravenous injection on day 22 after CIA induction.

Histological analysis

The lung tissues were fixed in 10% formalin, embedded in paraffin, and sectioned to 5 μm thickness using a microtome (Microm HM 325; Thermo Fisher Scientific, Waltham, MA, USA). The sections were stained with Masson's Trichrome and observed under a microscope at 200× magnification. Lung fibrosis was assessed at nine different sites in each lung section based on the modified Ashcroft and fibrosis scores (38). Briefly, the grading was scored on a scale of 0 (normal lung) to 8 (total fibrous obliteration of the field) for the Ashcroft score and 0 (no fibrosis) to 4 (fine connective fibrils in 100% of the area) for the fibrosis score. The percentages of collagen and alveolar spaces were measured using the ImageJ software (National Institutes of Health, Bethesda, MD, USA) and the final score of each section was the average of the scores for different sites.

Immunohistochemical and immunofluorescence staining

For immunohistochemistry, we used the VECTASTAIN Elite ABC Peroxidase Kit (catalog No. PK-6102; Vector Laboratories, Burlingame, CA, USA) and followed the manufacturer's protocol. Lung tissue slides were deparaffinized and stained with the anti-alpha smooth muscle actin (α-smooth muscle actin [SMA] 0.034 μg/ml, catalog No. ab7817; Abcam, Cambridge, UK) and anti-human nucleoli Ab (catalog No. ab190710; Abcam). Slides were incubated with biotinylated secondary Ab (catalog No. BA-9200; Vector Laboratories) and the 3,3′-diaminobenzidine (DAB) system (catalog No. D5697; Sigma-Aldrich, Saint Louis, MO, USA) was employed for color development. The α-SMA-positive area was quantified using the ImageJ software and the staining was normalized based on the average percentage of the α-SMA-positive area in the control group. Slides were analyzed at 200× magnification using the NIS-Elements software (Nikon, Tokyo, Japan) with a microscope imaging system (Nikon).

To conduct immunofluorescence staining for mitochondrial transfer analysis, the lung tissue sections were deparaffinized and incubated with primary Abs against cytochrome c oxidase subunit 4 (COX-4, catalog No. 4850; Cell Signaling Technology, Beverly, MA, USA) and surfactant protein C (SPC, catalog No. sc-518029; Santa Cruz Biotechnology, Dallas, TX,

USA) overnight at 4°C. The sections were then incubated with the secondary Abs (catalog No. A21206, anti-rabbit Alexa™ Fluor 488 or catalog No. A21203, anti-mouse Alexa Fluor™ 594; Thermo Fisher Scientific) for 2 h at 20–25°C. The sections were mounted using the ProLong® Gold Antifade Reagent containing 4′,6-diamidino-2-phenylindole (catalog No. P36935; Thermo Fisher Scientific). Representative images of COX-4- and SPC-positive cells were randomly visualized in four fields using a Nikon Eclipse Ni-U microscope (Nikon), following which the COX-4- and SPC-positive cells were counted.

Western blot analysis

Proteins were extracted from tissues and cells using radioimmunoprecipitation assay buffer (catalog No. 8900; Thermo Fisher Scientific) containing a cocktail of protease and phosphatase inhibitors (GenDEPOT, Baker, TX, USA). The protein lysates (20 µg) were separated using 10%–12% SDS-PAGE and transferred (100 volts, 90 min) onto polyvinylidene difluoride membranes (GE Healthcare, Solingen, Germany). Membranes were blocked using 5% skim milk with Tris-buffered saline containing 0.1% Tween 20 for 1 h and then probed with the primary Abs, anti-Miro-1 (catalog No. NBP1-89011; Novus Biologicals, Centennial, CO, USA), anti-Bcl-2 (catalog No. sc-7382; Santa Cruz Biotechnology), and anti-Bcl-2-associated X (Bax) (catalog No. sc-7480; Santa Cruz Biotechnology), overnight at 4°C. The membranes were incubated with horseradish peroxidase-conjugated secondary Abs (anti-rabbit, catalog No. 1706515 or anti-mouse, catalog No. 1706516; Bio-Rad, Hercules, CA, USA) for 1 h at 20–25°C. The signal was developed using an enhanced chemiluminescence western blotting substrate (Bio-Rad). Quantification was performed using the ImageJ software and normalized against β-actin.

Measurement of hydroxyproline levels

Hydroxyproline levels were measured using a Hydroxyproline Assay Kit (catalog No. 6017; Chondrex) according to the manufacturer's instructions. Briefly, 10 mg of mouse lung tissue was hydrolyzed overnight at 120°C with 100 µl of distilled water and 100 µl of 10 N HCl. The hydrolyzed sample was centrifuged at 9,425 ×g for 3 min, following which 10 µl of supernatant and 100 µl of 1× Chloramine T solution were added and the mixture was incubated for 20 min at 20–25°C. Thereafter, 100 µl of 1× DAB was added to the sample and the mixture was incubated for 30 min. Optical density was measured at a wavelength of 560 nm using a microplate reader (Molecular Devices, San Jose, CA, USA).

Quantitative real-time PCR

Total RNA was isolated from lung tissues using TRIzol™ reagent (Thermo Fisher Scientific) following the manufacturer's instructions. Subsequently, 1 µg of RNA was reverse transcribed into cDNA using the iScript™ cDNA Synthesis Kit (catalog No. 1708891; Bio-Rad). Real-time PCR was performed on a ViiA™ 7 Real-time PCR Detection System (Applied Biosystems, Foster City, CA, USA) using the TaqMan® Gene Expression Master Mix (catalog No. 4369016; Thermo Fisher Scientific). The relative expression levels of the target genes were determined using the $2^{-\Delta\Delta Ct}$ comparative method with glyceraldehyde 3-phosphate dehydrogenase as the internal reference gene. Mouse Taqman® assays (Applied Biosystems) were employed for the following genes: actin alpha 2, smooth muscle (*Acta2*, Mm00725412_s1), collagen type I alpha 1 chain (*Col1a1*, Mm00801666_g1), connective tissue growth factor (*Ctgf*, Mm01192933_g1), transforming growth factor-beta (*Tgfb1*, Mm01178820_m1), IL-1β (*Il1β*, Mm00434228 m1), and glyceraldehyde 3-phosphate dehydrogenase (*Gapdh*, Mm99999915_g1).

Flow cytometric analysis

Single cells from mouse lungs were isolated using a Lung Dissociation Kit (catalog No. 130-095-927, gentleMACS™; Miltenyi Biotec, Bergisch Gladbach, Germany) following the manufacturer's instructions. Briefly, PBS-washed lungs were transferred to a gentleMACS™ C tube containing the enzyme mix and dissociated using a gentleMACS™ Octo Dissociator with a heating function (catalog No. 130-096-427; Miltenyi Biotec). The resulting cell lysates were filtered through a 100 μm cell strainer and centrifuged at 500 ×g for 5 min. RBCs were removed by incubating the lysates with RBC lysis buffer (catalog No. 420301; BioLegend, San Diego, CA, USA) for 1 min, followed by centrifugation at 500 ×g for 5 min after the addition of PBS. Single lung cells were resuspended in PBS supplemented with 5 mM ethylenediaminetetraacetic acid and 2% FBS. Total cell counts were determined using a TC20 automated cell counter (Bio-Rad).

For flow cytometry analysis, 1×10^6 cells were incubated on ice with 100 μl of diluted Ab solution for 30 min. The following Abs were used: anti-CD45-BB515 (1:200, clone 30-F11, catalog No. 584590; BD Biosciences, San Jose, CA, USA), anti-CD11b-APC-Cy7 (1:200, clone M1/70, catalog No. 101226; BioLegend), anti-CD11c-BB700 (1:200, clone HL3, catalog No. 745899; BD Biosciences), anti-Ly-6C-BV605 (1:200, clone AL-21, catalog No. 563011; BD Biosciences), anti-CD4-PerCP-Cy5.5 (1:200, clone GK1.5, catalog No. 100434; BioLegend), anti-CD25-PE (1:200, clone PC61.5, catalog No. 12-0257-42; eBioscience, San Diego, CA, USA), anti-FoxP3-APC (1:200, clone FJK-16s, catalog No. 17-5773-82; eBioscience), anti-IFN-γ-FITC (1:200, clone XMG1.2, catalog No. 11-7311-82; eBioscience), and anti-IL-17A-APC (1:200, clone eBio17B7, catalog No. 17-7177-81; eBioscience). Stained samples were analyzed using an LSRFortessa™ X-20 flow cytometer (BD Biosciences) and data were analyzed using FlowJo version 10 (FlowJo, Ashland, OR, USA).

Cell culture and conditions of co-culture

DW-MSCs were cultured in StemPro™ MSC SFM XenoFree medium (Gibco BRL, Grand Island, NY, USA) supplemented with 1% L-glutamine (200 mM) and 1% penicillin-streptomycin. The culture medium was changed every 2–3 days and the cells were maintained under 5% CO_2 at 37°C. A549 cells (CCL-185, human type II AECs; ATCC, Gaithersburg, MD, USA) were cultured in DMEM supplemented with 10% FBS (Gibco BRL), 100 U/ml penicillin, and 100 mg/ml streptomycin. A549 cells were treated with 0 and 400 μM $CoCl_2$ (SHINYO Pure Chemical, Osaka Japan) for 24 h and co-cultured with or without DW-MSCs. For cell viability assay, western blot analysis, terminal deoxynucleotidyl transferase dUTP nick-end labeling (TUNEL) assay, and the mitochondrial respiration assay, DW-MSCs and A549 cells were indirectly co-cultured for 24 h using 0.4 μm Transwell™ inserts. For mitochondrial transfer analysis, DW-MSCs and A549 cells were directly co-cultured for 24 h.

Cell viability

To measure cell viability, we used the Cell Counting Kit-8 assay following the manufacturer's instructions (catalog No. CK04; Dojindo Laboratories, Kumamoto, Japan). Briefly, cells were incubated with Cell Counting Kit-8 reagent for 1 h and the absorbance was measured at 450 nm using a microplate reader. Each experiment was performed in triplicate.

TUNEL assay

The TUNEL assay was performed using the DeadEnd™ Colorimetric TUNEL System (catalog No. G7131; Promega, Madison, MI, USA) following the manufacturer's instructions. Briefly, cells were fixed with 4% paraformaldehyde and permeabilized. Subsequently, the cells were incubated with 100 μl of the TdT reaction mixture for 60 min in a humidified chamber

maintained at 37°C. The cells were developed with DAB Solution until a light-brown color developed. Stained cells were observed under a light microscope (Nikon) and images of 4–5 random fields were analyzed at an objective magnification of 200×. Cells exhibiting a brown color were counted as apoptosis-positive and their number was expressed as a percentage.

Assessment of mitochondria transfer

A549 cells were treated with 0 and 400 μM of $CoCl_2$ for 24 h. For immunofluorescence staining of tunneling nanotubes (TNTs), A549 cells and DW-MSCs were stained with CellTrace™ Violet (5 μM, 25 min, 37°C, catalog No. C34557; Invitrogen, Waltham, MA, USA) and MitoTracker™ Green FM (200 nM, 30 min, 37°C, catalog No. M7514; Invitrogen), respectively. The cells were then co-cultured for 24 h at a ratio of 1:1 and photographed under a fluorescence microscope (Nikon). Images were acquired using the NIS-Elements software and a Nikon microscope imaging system (Nikon). For the quantitative mitochondrial transfer assay, A549 cells were treated with 0 and 400 μM of $CoCl_2$ for 24 h followed by staining with CellTrace™ CFSE (5 μM, 30 min, 37°C, catalog No. C34554; Invitrogen). DW-MSCs were stained with MitoTracker™ Deep Red (5 μM, 30 min, 37°C, catalog No. M46753; Invitrogen). After washing, both cells were mixed at a 1:1 ratio and co-cultured for 0 or 24 h. The cells were then harvested and analyzed using an LSRForetessa™ X-20 flow cytometer. After gating only A549 cells expressing CellTrace™ CFSE, the ratio of A549 cells co-expressing CellTrace™ CFSE and MitoTracker™ Deep Red was analyzed using FlowJo version 10.

Mitochondrial respiration assay

Mitochondrial respiration was analyzed by measuring the oxygen consumption rate (OCR) with a Seahorse XFe96 Extracellular Flux Analyzer and XF Cell Mito Stress Test Kit (Agilent Technologies, Santa Clara, CA, USA) according to the manufacturer's instructions. The co-cultured cells were seeded at a density of 10,000 cells per 96-well Seahorse XF plate. After 24 h, the cells were washed once, and the growth medium was replaced with unbuffered XF DMEM (pH 7.4) supplemented with 25 mM D-glucose, 4 mM L-glutamine, and 1 mM sodium pyruvate. The OCR was measured under basal conditions and after sequential injection of 1.5 μM oligomycin, 2 μM FCCP, and 0.5 μM rotenone/antimycin. Data were analyzed using the Wave software (Agilent Technologies) and expressed as OCR in pmol/min/cell. All OCR values were normalized to the amount of protein obtained from each well after analysis.

Statistical analysis

Data visualization and analyses were performed using Prism versions 7 and 8 (GraphPad, San Diego, CA, USA). All data were analyzed using one-way analysis of variance followed by the Fisher's least significant difference test. p-values < 0.05 were considered significant. Data are expressed as mean ± SEM.

RESULTS

Establishment of the dosage, timing, and frequency of administration of DW-MSCs to BPF mice

The following experiments were conducted to determine the optimal dose, duration, and frequency of treatment with DW-MSCs to effectively treat pulmonary fibrosis in BPF mice. Fibrosis was assessed histologically in the lung tissues of mice at 4, 7, 14, and 21 days after BLM induction by comprehensively evaluating the Ashcroft score, fibrosis score, percentages of collagen deposition and alveolar space, and indicators of pulmonary fibrosis.

In our previous experiment, from the 4th day after BLM administration, fibrosis was observed in >20% of the total lung area of the mice and pulmonary fibrosis continued for up to 14 days after BLM induction; however, there was no change in the progression of pulmonary fibrosis from day 14 to day 21 (data not shown, unpublished). In particular, collagen deposition, which may reflect irreversible damage, was markedly increased on day 14 after BLM induction. Based on these results, to determine the optimal dose of DW-MSCs, a single injection of 1×10^5 or 1×10^6 DW-MSCs was administered on day 7 after BLM induction and pulmonary fibrosis in the mice was evaluated on day 21 (**Supplementary Fig. 1A**). DW-MSCs alleviated pulmonary fibrosis in BPF mice. BPF mice administered 1×10^6 DW-MSCs displayed improved pulmonary fibrosis compared with those administered 1×10^5 DW-MSCs (**Supplementary Fig. 1B and C**). Next, to determine the frequency of DW-MSC administration, single (on day 7) or serial (on days 7, 11, and 15) injections of 1×10^6 DW-MSCs were administered after BLM induction, and pulmonary fibrosis in the mice was evaluated on day 21 (**Supplementary Fig. 1D**). Both serial and single injections were found to improve pulmonary fibrosis in BPF mice to similar extents (**Supplementary Fig. 1E and F**).

DW-MSCs suppress pulmonary fibrosis in early-, active-, and chronic persistent-phase BPF mice

To investigate the potential therapeutic effects of DW-MSCs on early-phase pulmonary fibrosis in BPF mice, DW-MSCs were administered on the 4th day after BLM induction, following which fibrosis was evaluated in the lung tissue samples obtained from these mice on the 14th day (**Fig. 1A**). Compared with normal mice, BPF mice exhibited increased Ashcroft scores, fibrosis scores, and collagen content, as well as decreased alveolar space in the lung tissue. However, administration of DW-MSCs resulted in decreased Ashcroft scores, fibrosis scores, and collagen content, as well as increased alveolar space in the BPF mice (**Fig. 1B and C**). Furthermore, immunohistochemistry for α-SMA, a marker of myofibroblasts that plays an important role in the fibrosis process, revealed an increase in α-SMA-positive cells in BPF mice compared with normal mice. However, administration of DW-MSCs decreased the number of α-SMA-positive cells in BPF mice (**Fig. 1B and D**).

To investigate whether DW-MSCs improved active-phase pulmonary fibrosis in BPF mice, the mice were administered DW-MSCs on the 7th day after BLM induction, and fibrosis in the lung tissue was evaluated on day 21 (**Fig. 2A**). Compared with normal mice, BPF mice showed increased Ashcroft scores, fibrosis scores, and collagen content, and decreased alveolar space, which were considerably reversed upon DW-MSC treatment (**Fig. 2B and C**). Immunohistochemistry and western blot analysis revealed an increase in the number of α-SMA-positive cells in the lung tissues of BPF mice, which was reversed upon DW-MSC treatment (**Fig. 2D**). In addition, the increased hydroxyproline levels in BPF mice were downregulated by DW-MSCs (**Fig. 2E**). Next, to confirm the anti-fibrotic and anti-inflammatory roles of DW-MSCs in BPF mice, we examined the gene expression of *Acta2*, *Col1a1*, *Ctgf*, *Tgfb1*, and *Il1β*, and confirmed their reversal upon DW-MSC treatment (**Fig. 2F**). Furthermore, we explored the therapeutic effects of DW-MSCs in chronic persistent-phase BPF mice with repetitive BLM induction (**Fig. 3A**). BPF mice exhibited increased Ashcroft scores, fibrosis scores, collagen content, and reduced alveolar space, which were markedly ameliorated upon DW-MSC administration (**Fig. 3B and C**). In chronic persistent-phase BPF mice, a single injection of DW-MSCs improved pulmonary fibrosis, even under repetitive BLM induction. These results indicated that DW-MSCs inhibit pulmonary fibrosis in early-, active-, and chronic persistent-phase BPF mice.
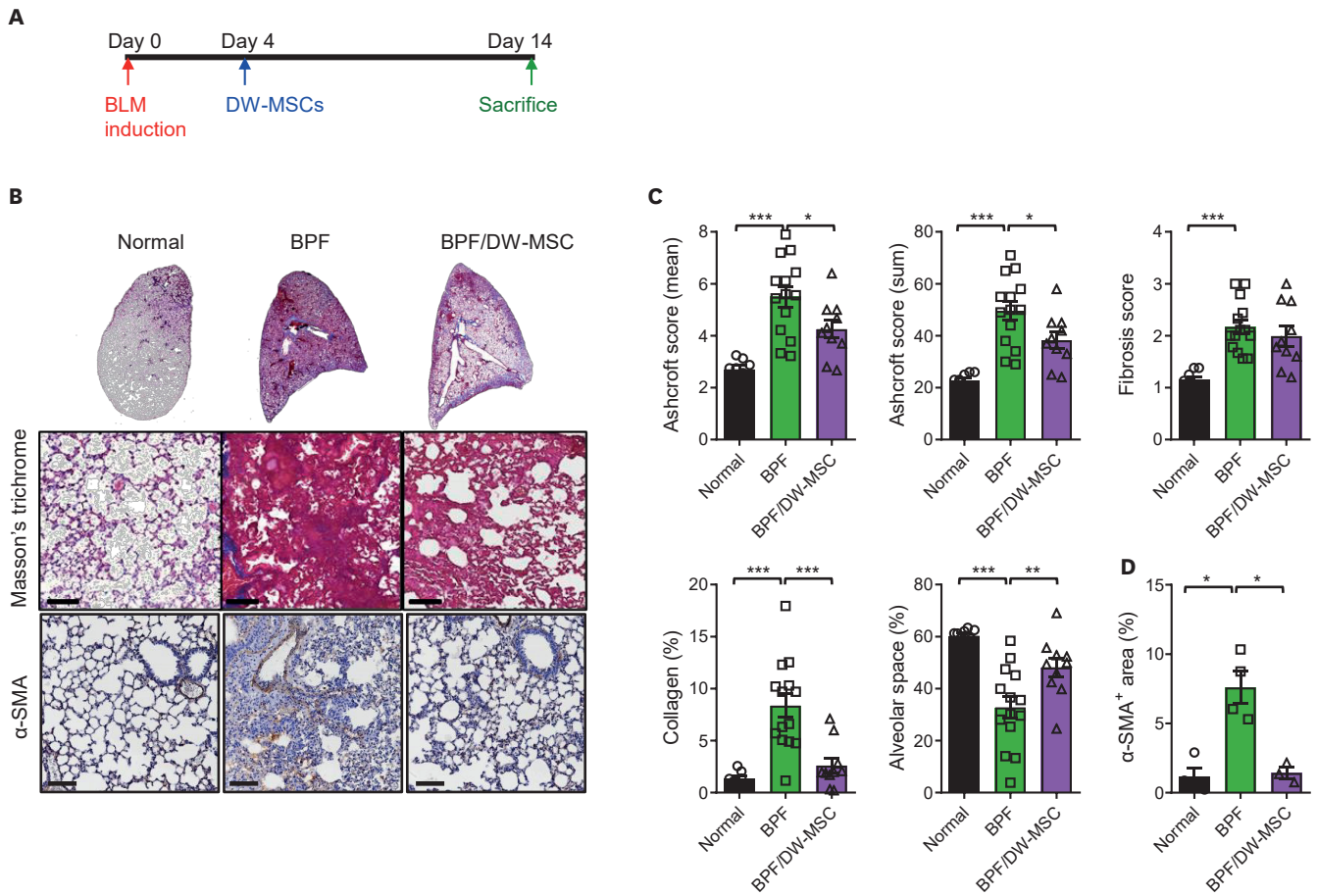
Figure 1. Effects of DW-MSCs on pulmonary fibrosis in early-phase BPF mice. (A) Experimental schedule schematic. (B) Representative images of the lung tissues from normal and BPF mice with or without DW-MSC treatment stained with Masson's Trichrome (magnification: 40× and 200×) and of lung sections immunohistochemically stained for α-SMA (magnification: 400×). (C) Semiquantitative assessment of lung fibrosis in terms of the Ashcroft score, fibrosis score, percentages of collagen content, and alveolar space. The data are cumulative results from three independent experiments, with a total of 8–14 mice/group. (D) Semiquantitative assessment of the α-SMA-positive area in the lung. The data are from 3–4 mice/group, where each symbol represents one mouse. Scale bar: 50 μm ± SEM.
Statistical significance was determined using one-way analysis of variance followed by Fisher's least significant difference. All data are presented as mean ± SEM (*p<0.05, **p<0.01, and ***p<0.001 vs. normal).

DW-MSCs produce an effect that is comparable to that of established antifibrotic agents (nintedanib and pirfenidone)

To further establish the efficacy of DW-MSCs, a comparative analysis was performed with nintedanib, an existing treatment for pulmonary fibrosis (**Fig. 4A**). DW-MSCs alleviated fibrosis in the lungs of BPF mice to a level comparable with that observed with nintedanib; they also downregulated the collagen content more effectively than nintedanib (**Fig. 4B and C**). Immunohistochemical analysis showed that DW-MSCs reduced the number of α-SMA-positive cells in the lungs of BPF mice to a level similar to that observed with nintedanib (**Fig. 4B and D**). Furthermore, we confirmed that human nucleoli-positive cells were observed only in the lung tissues of BPF mice administered DW-MSCs (**Fig. 4B and C**). Next, we compared the efficacy of DW-MSCs to that of pirfenidone (**Fig. 4E**). DW-MSCs improved pulmonary fibrosis in BPF mice to an extent similar to that observed with pirfenidone (**Fig. 4F and G**). We found that DW-MSCs reduced the collagen content more effectively than nintedanib or pirfenidone (**Fig. 4C and G**).
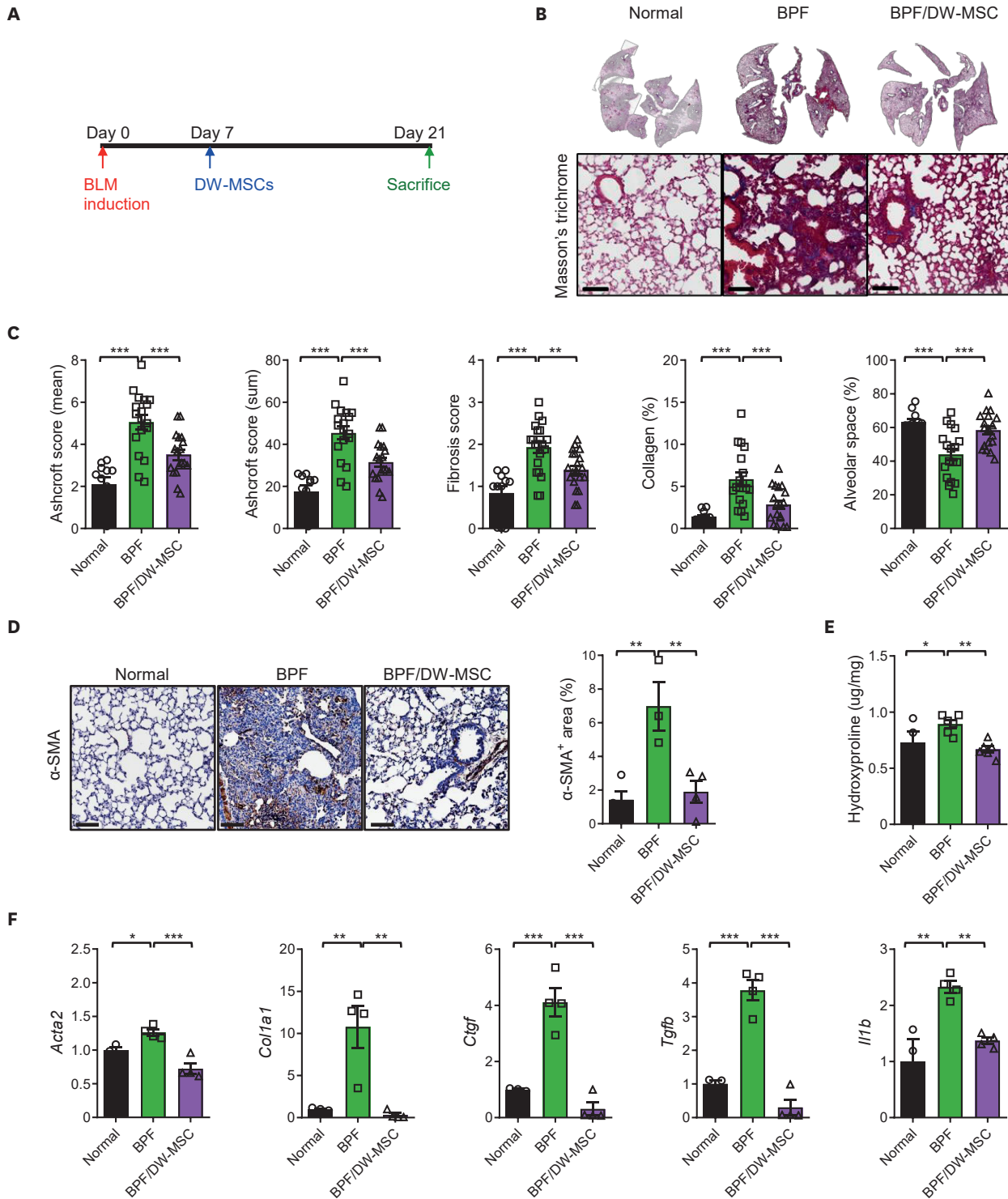
Figure 2. Effects of DW-MSCs on pulmonary fibrosis in active-phase BPF mice. (A) Experimental schedule schematic. (B) Representative images of Masson's Trichrome-stained lung tissues from normal and BPF mice with/without DW-MSC treatment (magnification: 40× and 200×). (C) Semiquantitative assessment of lung fibrosis in terms of the Ashcroft score, fibrosis score, as well as percentages of collagen content and the alveolar space. (D) Representative images of lung tissue sections immunohistochemically stained for α-SMA (magnification, 200×) and semiquantitative assessment of the α-SMA-positive area in the lung. (E) Semiquantitative assessment of hydroxyproline and (F) expression profiles of pro-fibrotic and pro-inflammatory genes in the lung (n=3–4 mice/group); each symbol represents one mouse. (B-C) Cumulative data from three independent experiments were used for a total of 11–18 mice/group. Scale bar: 50 μm. Statistical significance was determined using one-way analysis of variance followed by Fisher's least significant difference (*p<0.05, **p<0.01, and ***p<0.001 vs. normal).
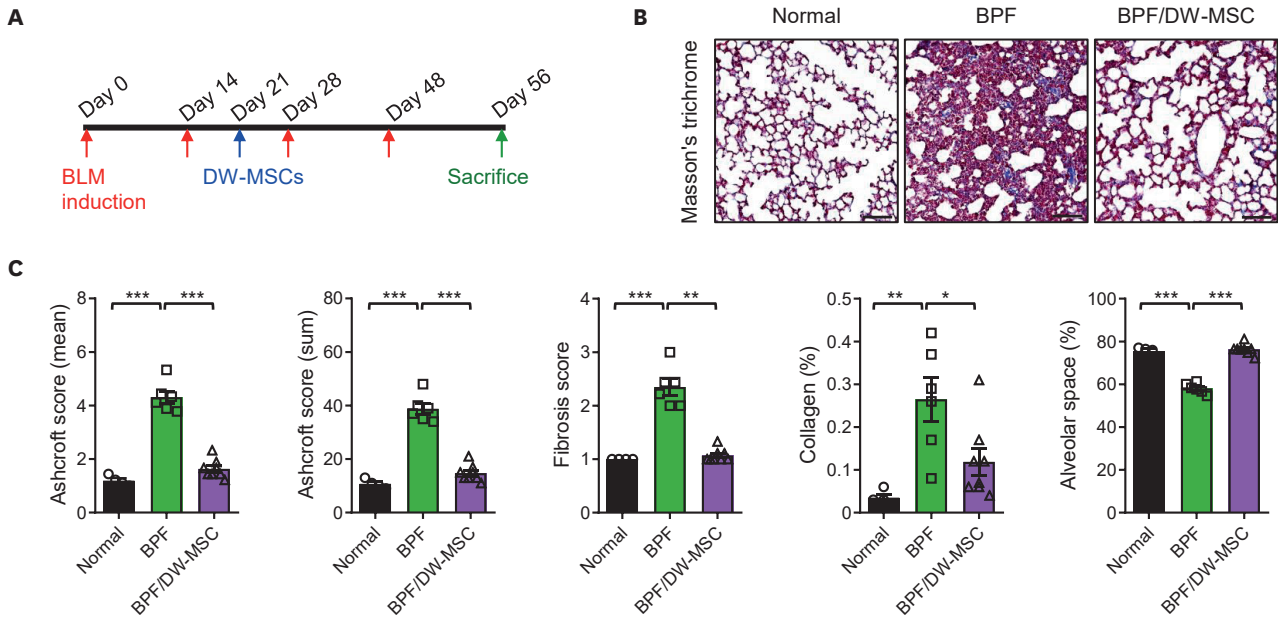
IMMUNE NETWORK

Figure 3. Effects of DW-MSCs on pulmonary fibrosis in mice with chronic persistent-phase BPF. Mice were given a total of four doses of BLM every other week for 8 weeks, following which 1×10⁶ DW-MSCs were administered to the mice at 3 wk after BLM induction, and pulmonary fibrosis was assessed 2 weeks after the last BLM induction. (A) Experimental schedule schematic. (B) Representative images of Masson's Trichrome-stained lung tissues of normal and BPF mice with or without DW-MSC treatment (magnification, 200×). (C) Quantitative assessment of pulmonary fibrosis in terms of the Ashcroft score, fibrosis score, and percentages of collagen content and alveolar space (n=4–8 mice/group). Scale bar: 100 μm.
Each symbol represents a single mouse. *p<0.05, **p<0.01, and ***p<0.001 vs. normal.

DW-MSCs have a therapeutic effect against pulmonary fibrosis in CIA mice

To investigate whether DW-MSCs improve pulmonary fibrosis in CIA mice, we administered a single dose of 1×10⁶ DW-MSCs on day 22 after CIA induction and evaluated fibrosis in the lung tissues of CIA mice on day 35 (**Supplementary Fig. 2A**). In our preliminary study, inflammation and fibrosis progression in the entire lung tissue was confirmed on day 22 after CIA induction, which continued to increase until day 29 before decreasing. On day 42, pulmonary fibrosis showed an overall improvement (data not shown). Compared to normal mice, CIA mice displayed increased pulmonary fibrosis, which was significantly reduced upon DW-MSC treatment (**Supplementary Fig. 2B and C**). Immunohistochemical analysis of α-SMA showed an increase in α-SMA-positive cells in CIA mice compared with that in normal mice, which decreased significantly upon DW-MSC treatment (**Supplementary Fig. 2D**). These results indicated that DW-MSCs inhibited pulmonary fibrosis in CIA mice.

DW-MSCs suppress lung fibrosis through the regulation of immune cells in BPF mice

To investigate whether DW-MSCs are involved in immune cell modulation in BPF mice, we administered DW-MSCs (1×10⁶) at 4 days after BLM induction and performed flow cytometry analysis of the lung tissues on days 7 and 14 (**Fig. 5A**). Seven days after BLM induction, the number of B cells (B220⁺ B cells among CD45⁺ cells) in the lungs of BPF mice increased by approximately 20% compared with that in the lungs of normal mice, but decreased upon treatment with DW-MSCs (**Fig. 5B**). Fourteen days after BLM treatment, an imbalance in Th17 (CD4⁺ IL-17A⁺) and Treg (CD4⁺ FoxP3⁺ CD25⁺) cells was observed in the lungs of BPF mice, which was restored upon treatment with DW-MSCs (**Fig. 5C**).
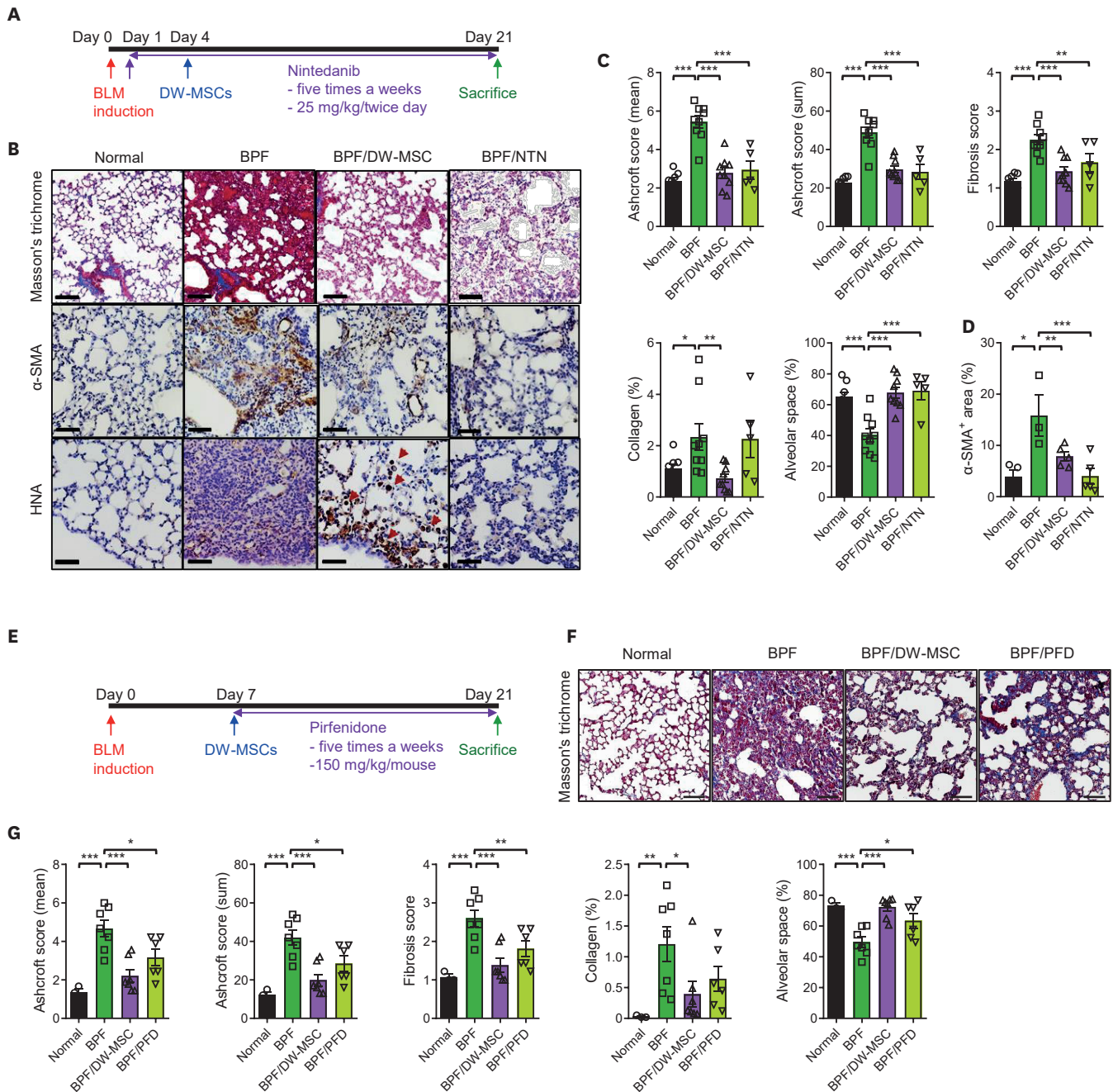
Figure 4. Comparative therapeutic effects of DW-MSCs and NTN or PFD on pulmonary fibrosis in BPF mice. BPF mice were intravenously injected with DW-MSCs (2×10^6) on Day 4 or administered NTN (50 mg/kg) daily for 3 weeks, following which the mice were sacrificed on Day 21. (A) Experimental schedule schematic. (B) Representative images of lung tissues stained with Masson's Trichrome, α-SMA, and HNA (magnification: 200×). (C) Semiquantitative assessment of lung fibrosis in terms of the Ashcroft score, fibrosis score, and percentages of collagen content and alveolar space. (n=3–8 mice/group). (D) Semiquantitative assessment of the α-SMA-positive area in the lungs of normal and BPF mice with/without DW-MSC or NTN treatment (n=3–5/group). Mice were intravenously injected with DW-MSCs (1×10^6) on Day 7 or pirfenidone (150 mg/kg/d) was administered daily to the mice for 3 weeks, following which they were sacrificed on day 21. (E) Experimental schedule schematic. (F) Representative images of lung tissues stained with Masson's Trichrome. (G) Semiquantitative assessment of lung fibrosis in terms of the Ashcroft score, fibrosis score, and percentages of collagen content and alveolar space (n=3–8 mice/group); each symbol represents one mouse. Scale bar: 50 μm.

NTN, nintedanib; PFD, pirfenidone; HNA, human nuclear Ag.

Statistical significance was determined using one-way analysis of variance followed by Fisher's least significant difference (*$p < 0.05$, **$p < 0.01$, and ***$p < 0.001$ vs. normal).
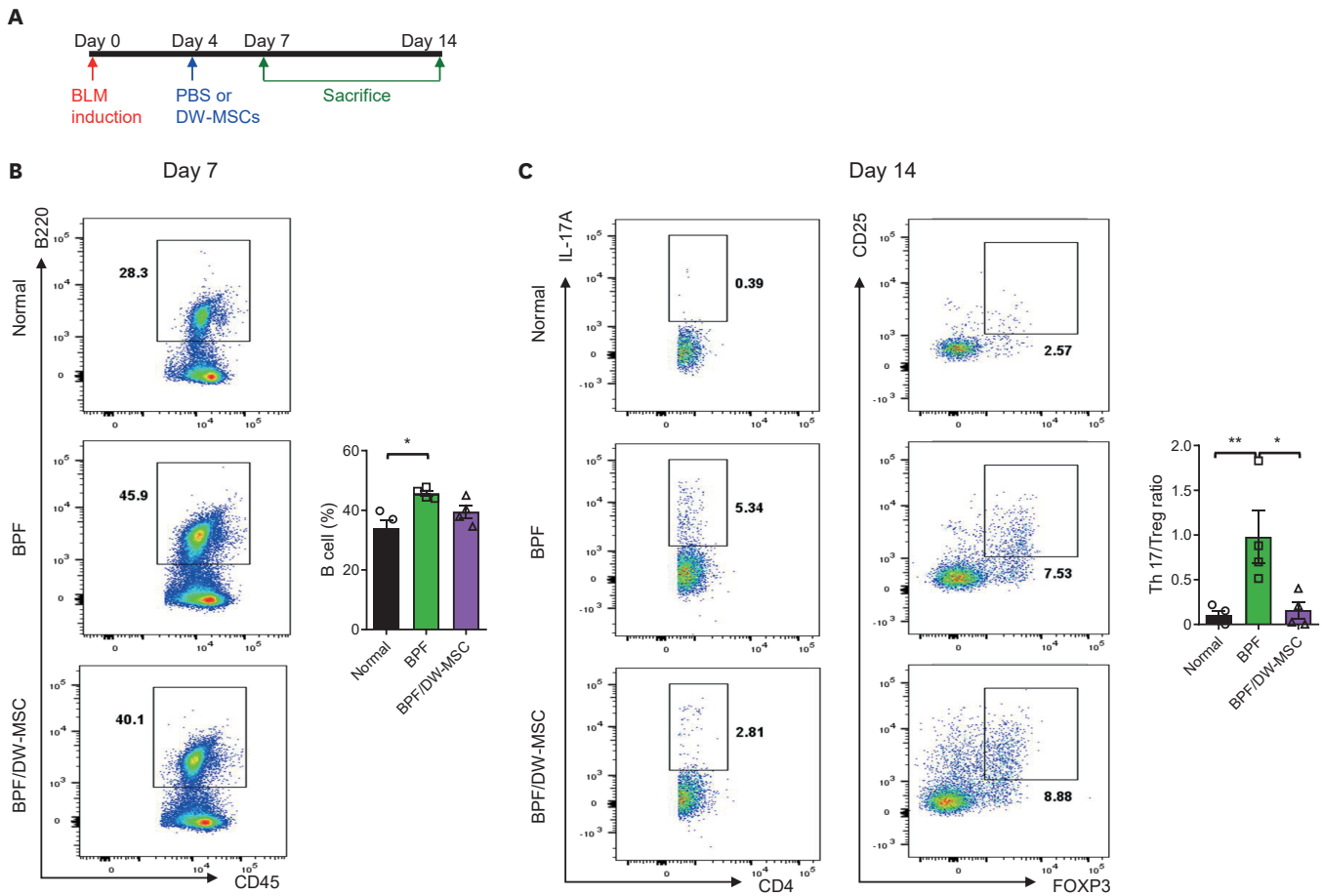
Figure 5. Effects of DW-MSCs on immune cell populations in the lung tissues of BPF mice. (A) Experimental schedule schematic. (B) Flow cytometry analysis of lung tissues of BPF mice at 7 d after BLM induction showed an up to 20% increase in the number of B cells (B220+ B cells among CD45+ cells) compared with that in normal mice; this increase was decreased upon treatment with DW-MSCs. (C) At 14 d after BLM induction, an imbalance in Th17 (CD4+ IL-17A+) and Treg (CD4+ FoxP3+ CD25+) cells was observed in the lungs of BPF mice, which was restored by treatment with DW-MSCs. The gating strategy is presented in **Supplementary Fig. 4** (n=4 mice/group for normal and BPF mice with or without DW-MSC treatment); each symbol represents one mouse.
Statistical significance was determined using one-way analysis of variance followed by Fisher's least significant difference (*p<0.05 and **p<0.01 vs. normal).

DW-MSCs mitigate CoCl₂-induced apoptosis in AECIIs

After treatment with 400 μM $CoCl_2$ for 24 h, the A549 cells displayed significantly lower cell viability than untreated cells; however, co-culture with DW-MSCs significantly increased the viability of A549 cells from 54.6% to 77.2% (**Fig. 6A**). In western blot analysis, A549 cells treated with 400 μM $CoCl_2$ showed downregulation of Bcl-2 expression and upregulation of Bax expression. However, co-culture with DW-MSCs reversed these effects, leading to increased Bax expression and decreased Bcl-2 expression (**Fig. 6B**). Analysis of apoptosis using TUNEL staining revealed a significant increase in apoptotic cells among A549 cells treated with 400 μM $CoCl_2$ compared to that among untreated A549 cells (0 μM $CoCl_2$) (**Fig. 6C**). However, co-culturing with DW-MSCs reduced $CoCl_2$-induced apoptosis in A549 cells. These results suggested that DW-MSCs exert a protective effect against $CoCl_2$-induced apoptosis in A549 cells.

DW-MSCs improve respiratory function via mitochondrial transfer into AECIIs

Using fluorescence microscopy, we observed the migration of mitochondria from DW-MSCs to A549 cells through TNTs (**Fig. 7A**). Furthermore, we found an increased mitochondrial transfer ratio of DW-MSCs to damaged A549 cells compared to healthy A549 cells (**Fig. 7B**). A549 cells
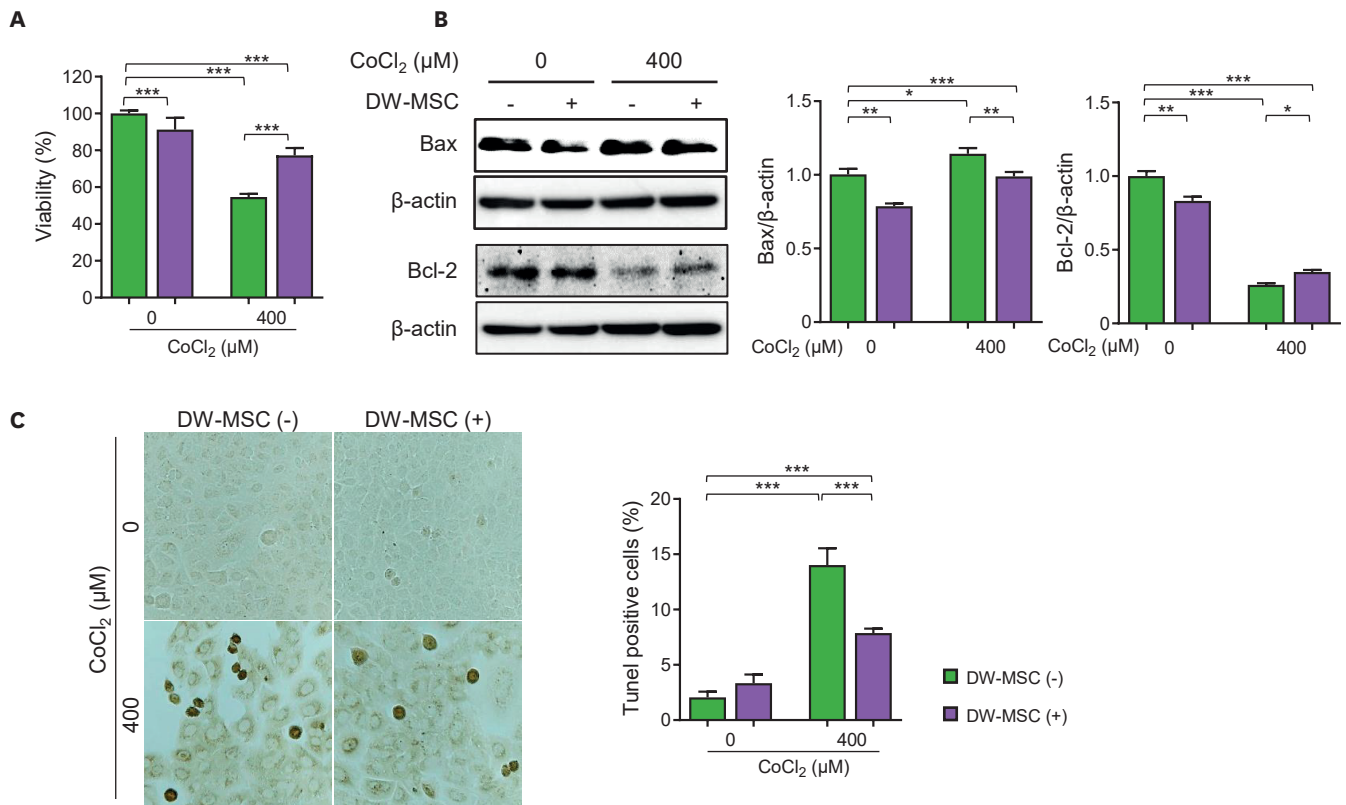
Figure 6. Effects of DW-MSCs on CoCl₂-induced apoptosis in A549 cells. CoCl2-induced A549 cells were co-cultured with or without DW-MSCs for 24 h in a hypoxic condition and the cell viability of the AECs and levels of apoptosis in them were assessed. (A) Quantitative analysis of A549 cell viability. (B) Expression of Bax and Bcl-2 proteins in A549 cells. Full-length blots/gels are presented in **Supplementary Fig. 5**. (C) Representative images of the TUNEL assay and percentage of TUNEL-positive cells (n=3 experiments/group).
***$p < 0.001$ vs. A549 cells (without CoCl₂ and DW-MSCs).

damaged by CoCl₂ exhibited a significant reduction in basal respiration, maximal respiration, proton peak, and ATP production compared to healthy A549 cells (**Fig. 7C**). However, co-culture with DW-MSCs significantly improved the overall mitochondrial respiration in the damaged A549 cells, as evidenced by the increase in basal respiration, maximal respiration, proton peak, and ATP production across all indices. We observed the expression of human nuclear-encoded subunit 4 of cytochrome c oxidase (hCOX-4) in SPC-positive AECIIs in BPF mice (**Fig. 8**), which suggested that the mitochondria of human-origin DW-MSCs migrated to mouse AECIIs.

Miro-1 exhibited minimal to negligible expression in bone marrow-MSCs and umbilical cord-MSCs by passage 6. Interestingly, DW-MSCs exhibited robust Miro 1 expression as early as passage 13. Subsequent exposure to IFN-γ stimulation confirmed sustained upregulation of Miro-1 expression persisting through passage 18 (**Supplementary Fig. 3**).

DISCUSSION

In this study, we found that DW-MSCs with high clinical potency consistently exhibited favorable therapeutic effects in the early, active, and chronic persistent-phases of mouse ILD models. The therapeutic potential of a single intravenous administration of DW-MSCs was comparable to that of nintedanib or pirfenidone, both of which require daily oral
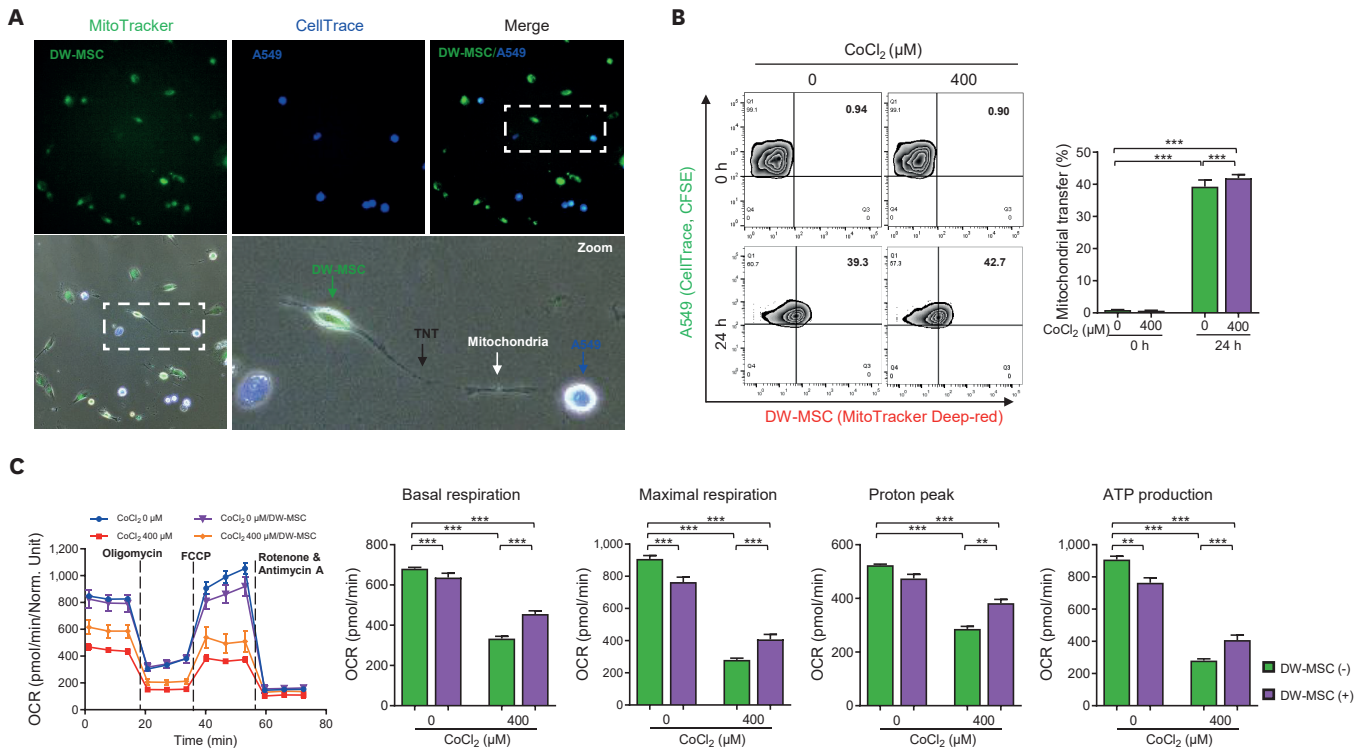
Figure 7. Modulatory effects of DW-MSC mitochondrial transfer and respiration of hypoxia-induced A549 cells. A549 cells were co-cultured with/without DW-MSCs for 24 h in a hypoxic condition. (A) Representative images showing TNT connections (arrows) between DW-MSCs and hypoxia-induced A549 cells. (B) Representative distribution of co-cultured CFSE-labeled A549 cells and MitoTracker™-labeled DW-MSCs, analyzed using fluorescence-activated cell sorting, and the time-course of the mitochondrial transfer ratio for transfer between DW-MSCs and hypoxia-induced A549 cells (n=3 experiments/group). (C) Mitochondrial respiration was analyzed in hypoxia-induced A549 cells. Overall mitochondrial OCRs were measured after injection of oligomycin (1.5 μM), FCCP (2 μM), and rotenone/antimycin A (0.5 μM). Quantitative assessment of respiration, proton peak, and ATP production (n=6 experiments/group). Statistical significance was determined using one-way analysis of variance followed by least significant difference. Data are presented as mean ± SEM.
FCCP, carbonyl cyanite-4 phenylhydrazone.
**p<0.01 and ***p<0.001 vs. A549 cells (without CoCl₂ and DW-MSCs).

administration. DW-MSCs inhibited apoptosis in damaged AECIIs and enhanced cell viability and mitochondrial respiration through mitochondrial transfer. Furthermore, DW-MSCs exhibited immunomodulatory effects by influencing B cells during the early phase and promoting an increase in Treg cells and a decrease in Th17 cells during the chronic persistent-phase. In addition, they reduced the expression of various inflammatory- and fibrosis-related genes and proteins. Together, our results suggest that administration of DW-MSCs could serve as a novel therapeutic approach in the treatment of ILD.

MSCs have been found to have therapeutic effects in many animal models of ILD (23). As a result, adult tissue-origin MSCs such as bone marrow-MSCs and umbilical cord-MSCs are currently being evaluated in early clinical studies to examine their safety and efficacy in IPF patients (29-31). In comparison, our study suggests that embryonic-origin DW-MSCs show potential in clinical settings with regard to several aspects. First, in most of the previous studies, the passage number of adult tissue-origin MSCs was less than 6–7 (39-41), whereas in the present study, we used passage-13 and -14 DW-MSCs to confirm the efficacy in ILD mice models. This illustrates that DW-MSCs, derived from embryonic stem cells with a greater expansion capacity, have the potential for commercialization as stem cell therapeutics. Second, in most of the previous studies, MSCs were primarily administered during the early phase of BPF in mouse models and in the chronic phase in only a few (23,42,43). However,
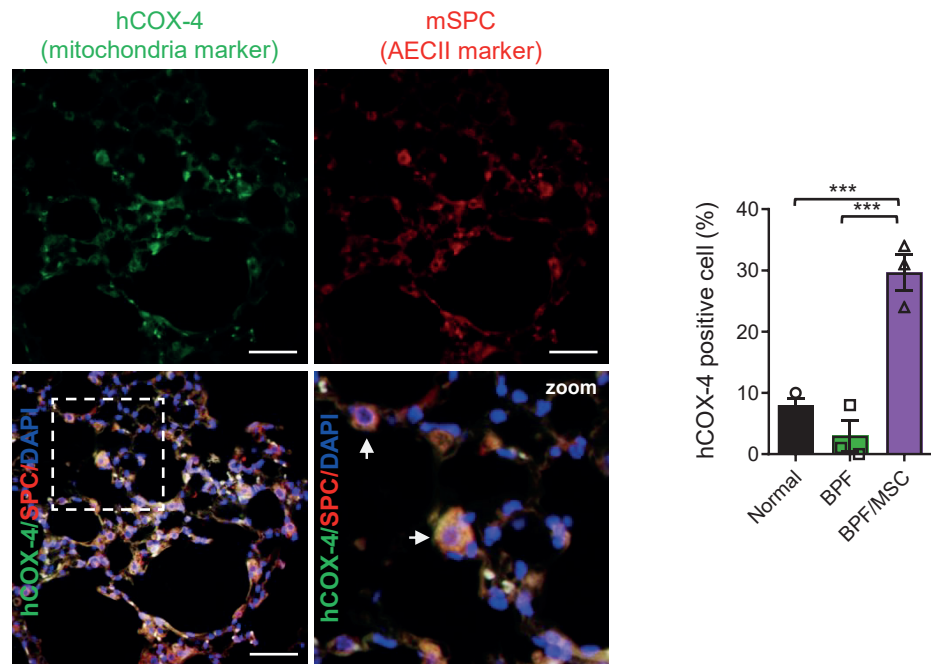
Figure 8. Effects of DW-MSCs on mitochondria transfer to AEC IIs in the lungs of active BPF mice. Representative images of lung tissues stained with hCOX-4 (human specific mitochondria marker; green) and mSPC (ACEII marker; red) n=3 mice/group (normal and BPF mice with/without DW-MSC treatment); each symbol represents one mouse. Statistical significance was determined using one-way analysis of variance followed by least significant difference. Data are presented as mean ± SEM.
mSPC, mouse surfactant protein c/SPC.
***p<0.001 vs. normal.

our findings demonstrate the effects of DW-MSCs in the early, active, and chronic persistent-phases of BFP. Third, our study extended beyond BPF to a CIA model of pulmonary fibrosis, showing that DW-MSCs hold therapeutic potential not only for IPF but also for CTD-ILD. These results indicate a promising future for DW-MSCs in clinical trials and their potential practical use as a treatment option for various forms of ILD.

Recently, pirfenidone and nintedanib have been used to treat ILD, which demonstrates their ability to delay the decline in the lung function (15,16). In the present study, we compared these 2 drugs with DW-MSCs and confirmed their similar therapeutic effects. However, DW-MSCs have two advantages as therapeutic agents over nintedanib and pirfenidone. First, DW-MSCs need to be administered only once to achieve similar therapeutic effects, whereas nintedanib and pirfenidone need to be administered daily. Second, nintedanib and pirfenidone are associated with numerous side effects, thereby posing challenges in their administration. For example, 95.2% of patients taking nintedanib report diarrhea and nearly 30% report frequent occurrences of nausea and dyspepsia along with skin rash (15,16). In contrast, a recent study evaluating the safety of DW-MSCs administered to patients with COVID-19 showed a low incidence of adverse events (37). Therefore, owing to their fewer administration requirements and a lower incidence of side effects, DW-MSCs are expected to be utilized in combination with existing treatments or as therapeutic options for ILD in the future.

Several studies have shown that MSC treatment reduces the expression of inflammatory and pro-fibrotic cytokines and as a result improves the BLM-induced lung tissue inflammatory response and fibrosis (23,24). Recent studies have also identified the involvement of immune

cells such as T and B cells in the pathogenesis of ILD; these cells have varying importance depending on the disease phase (11). Moreover, studies have shown that MSCs can alleviate fibrosis through the modulation of a subset of immune cells in liver fibrosis and chronic cigarette smoking-induced lung inflammation (44,45). In the present study, DW-MSCs inhibited the expression of fibrosis or inflammation-related genes such as *Tgfb1* and *Il1β* in BPF mice. Additionally, during the early phase, DW-MSCs inhibited B cells whereas during the active phase they suppressed Th17 cells. These findings demonstrate that DW-MSCs can be utilized for the treatment of ILD owing to their anti-inflammatory and immunomodulatory effects.

Recent studies have shown that restoration of AECII mitochondrial dysfunction can subsequently lead to a reduction in pulmonary inflammation and fibrosis and that MSCs exert a protective effect on lung tissues by inhibiting the apoptosis of AECIIs through the transfer of healthy mitochondria of MSCs into damaged AECIIs (25-28). In the present study, DW-MSCs reduced hypoxia-induced apoptotic gene expression and improved the cell viability of AECIIs. Furthermore, damaged AECIIs experienced mitochondrial dysfunction and DW-MSCs facilitated the transfer of mitochondria to damaged cells leading to the restoration of mitochondrial respiration in AECIIs. Moreover, DW-MSCs exhibited an advantage over adult tissue-derived MSCs in maintaining mitochondrial transfer protein Miro-1 expression. Overall, these findings suggest that DW-MSCs possess a prolonged capacity for mitochondrial transfer particularly in hypoxic environments of ILD and thus improve damaged AECIIs and lung fibrosis.

This study has a limitation in that it does not fully explain the lack of significant difference in the efficacy of DW-MSCs administered in different numbers and injection frequencies on BPF mice. While experiments using animal models of non-inflammatory and degenerative diseases, such as spinal cord injury or cerebral ischemia, have shown the benefits of higher doses or repeated administration of MSCs, no additional therapeutic effect has been observed in mouse models of RA (46-48). This may be attributed to MSCs losing their immunomodulatory properties and becoming pro-inflammatory upon prolonged exposure to inflammatory microenvironments (49,50). Although further research is needed to have a clear understanding of this, it is suggested that the lack of therapeutic benefit of higher doses or repeated administration of DW-MSCs may be due to similar persistent inflammatory characteristics in IPF and RA.

Our study provides compelling evidence of the therapeutic potential of a single injection of DW-MSCs in improving IPF and CTD-ILD. These effects are achieved through the protection of AECIIs by inhibiting apoptosis, facilitating mitochondrial transfer, and exerting anti-inflammatory and immunomodulatory effects (**Fig. 9**). Their high clinical applicability and minimal side effects are added advantages. Thus, DW-MSCs are ideal candidates for future ILD cellular therapeutics.
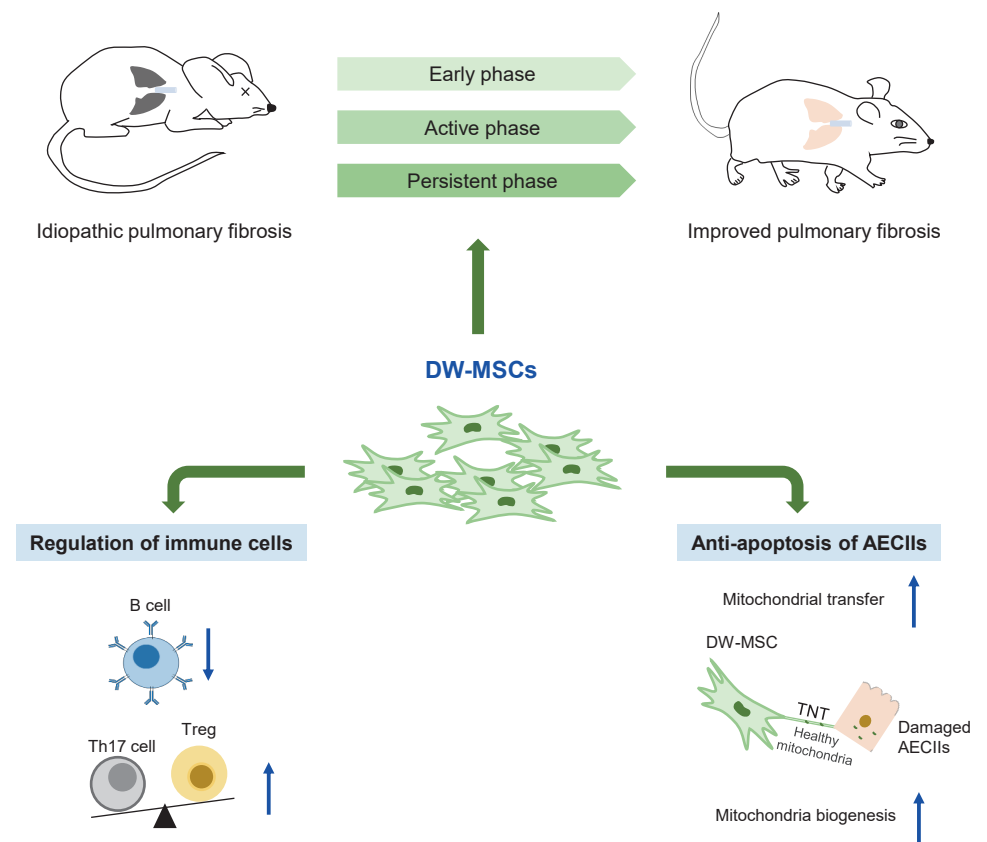
ACKNOWLEDGEMENTS

Figure 9. Summarized figure of the therapeutic efficacy and mode of action of DW-MSCs in idiopathic pulmonary fibrosis.

SUPPLEMENTARY MATERIALS

Supplementary Figure 1

Effects of injection with different cell numbers of DW-MSCs in the active-phase BPF mice. (A, D) Experimental schedule schematic. (B, C) BPF mice were injected with two different cell numbers (1×10^5 or 1×10^6) of DW-MSCs on Day 7 and sacrificed on Day 21. (B) Representative images of Masson's Trichrome-stained lung tissues of normal and BPF mice with or without DW-MSC treatment (magnification, 40×). (C) Semiquantitative assessment of lung fibrosis in terms of the Ashcroft score, fibrosis score, and percentages of collagen content and alveolar space. <underline>n</underline>=3–6 mice/group. (E, F) BPF mice were injected with DW-MSCs (1×10^6) once on day 7 (single injection) or three times on Days 7, 11, and 15 (serial injections) and sacrificed on Day 21. (E) Representative images of Masson's Trichrome-stained lung tissues of normal and BPF mice with or without DW-MSC treatment (magnification, 40×). (F) Quantitative assessment of pulmonary fibrosis in terms of the Ashcroft score, fibrosis score, and percentages of collagen content and alveolar space. n=3–6 mice/group; each symbol represents one mouse.

Click here to view

Supplementary Figure 2

Effects of DW-MSCs on pulmonary fibrosis in CIA mice. CIA mice were injected with DW-MSCs ($1×10^6$) on Day 22 and sacrificed on Day 35. (A) Experimental schedule schematic. (B) Representative images of Masson's Trichrome-stained lung tissues (magnification, 40× and 200×). Semiquantitative assessment of (C) lung fibrosis in terms of the Ashcroft score, fibrosis score, and percentages of collagen content and alveolar space and (D) the α-SMA-positive area in the lungs of normal and CIA mice with or without DW-MSCs. n=3–6 mice/group for normal and CIA mice with or without DW-MSC treatment. Each symbol represents one mouse.

Click here to view

Supplementary Figure 3

Comparison of the expression of Miro-1 protein in DW-MSCs, BM-MSCs, and UC-MSCs. (A) BM-MSCs and UC-MSCs were provided by Professor Lee, College of Veterinary Medicine, Gyeongsang National University. DW-MSCs, BM-MSCs, and UC-MSCs at various passages were stimulated with or without IFN-γ for 48 h, following which western blot was performed to confirm the protein expression of Miro-1. β-actin was used as the loading control. (B) Full-length blots/gels.

Click here to view

Supplementary Figure 4

Gating strategy for Th17, Treg, and B cells. Doublet cells and debris were eliminated by gating in the FSC-A vs. FSC-H and FSC-A vs. SSC-A plots. Dead cells were discriminated by staining with a viability dye. (A) CD4+ T cells were distinguished by staining for CD3 and CD4. Th17 cells were identified by positive staining for IL-17A and CD4+. (B) Tregs were identified by positive staining for CD25+ and Foxp3+ in the CD4+ T cell population. (C) Total immune cells were identified based in CD45 expression. Negative staining of the Ly6G population was used to exclude non-neutrophils. Myeloid and lymphoid leukocytes were distinguished by staining for CD11b and CD11c. Positive staining of B220 CD11b and CD11c negative population was used to identify B cells.

Click here to view

Supplementary Figure 5

Full-length blots/gel of Bax and Bcl-2 used in the western blot analysis of hypoxia-induced A549 cells. A549 cells were stimulated with 0 or 400 μM $CoCl_2$ for 24 h and co-cultured with or without DW-MSCs. Western blotting was conducted to analyze the expression of Bax and Bcl-2 proteins. β-actin was used as the loading control.

Click here to view

REFERENCES

1. Raghu G, Rochwerg B, Zhang Y, Garcia CA, Azuma A, Behr J, Brozek JL, Collard HR, Cunningham W, Homma S, et al. An official ATS/ERS/JRS/ALAT clinical practice guideline: treatment of idiopathic pulmonary fibrosis. An update of the 2011 clinical practice guideline. *Am J Respir Crit Care Med* 2015;192:e3-e19.
   PUBMED | CROSSREF

2. Raghu G, Remy-Jardin M, Myers JL, Richeldi L, Ryerson CJ, Lederer DJ, Behr J, Cottin V, Danoff SK, Morell F, et al. Diagnosis of idiopathic pulmonary fibrosis. An official ATS/ERS/JRS/ALAT clinical practice guideline. *Am J Respir Crit Care Med* 2018;198:e44-e68.
   PUBMED | **CROSSREF**

3. du Bois RM. An earlier and more confident diagnosis of idiopathic pulmonary fibrosis. *Eur Respir Rev* 2012;21:141-146.
   PUBMED | **CROSSREF**

4. Song JW. Interstitial lung disease in connective tissue disease. *J Rheum Dis* 2014;21:282-288.
   CROSSREF

5. Park JH, Kim DS, Park IN, Jang SJ, Kitaichi M, Nicholson AG, Colby TV. Prognosis of fibrotic interstitial pneumonia: idiopathic versus collagen vascular disease-related subtypes. *Am J Respir Crit Care Med* 2007;175:705-711.
   PUBMED | **CROSSREF**

6. Spagnolo P, Lee JS, Sverzellati N, Rossi G, Cottin V. The lung in rheumatoid arthritis: focus on interstitial lung disease. *Arthritis Rheumatol* 2018;70:1544-1554.
   PUBMED | **CROSSREF**

7. Tsuchiya Y, Takayanagi N, Sugiura H, Miyahara Y, Tokunaga D, Kawabata Y, Sugita Y. Lung diseases directly associated with rheumatoid arthritis and their relationship to outcome. *Eur Respir J* 2011;37:1411-1417.
   PUBMED | **CROSSREF**

8. Wynn TA. Integrating mechanisms of pulmonary fibrosis. *J Exp Med* 2011;208:1339-1350.
   PUBMED | **CROSSREF**

9. Raghu G, Collard HR, Egan JJ, Martinez FJ, Behr J, Brown KK, Colby TV, Cordier JF, Flaherty KR, Lasky JA, et al. An official ATS/ERS/JRS/ALAT statement: idiopathic pulmonary fibrosis: evidence-based guidelines for diagnosis and management. *Am J Respir Crit Care Med* 2011;183:788-824.
   PUBMED | **CROSSREF**

10. Khanna D, Lin CJ, Furst DE, Wagner B, Zucchetto M, Raghu G, Martinez FJ, Goldin J, Siegel J, Denton CP. Long-term safety and efficacy of tocilizumab in early systemic sclerosis–interstitial lung disease: open-label extension of a phase 3 randomized controlled trial. *Am J Respir Crit Care Med* 2022;205:674-684.
    PUBMED | **CROSSREF**

11. Heukels P, Moor CC, von der Thüsen JH, Wijsenbeek MS, Kool M. Inflammation and immunity in IPF pathogenesis and treatment. *Respir Med* 2019;147:79-91.
    PUBMED | **CROSSREF**

12. Holroyd CR, Seth R, Bukhari M, Malaviya A, Holmes C, Curtis E, Chan C, Yusuf MA, Litwic A, Smolen S, et al. The British Society for Rheumatology biologic DMARD safety guidelines in inflammatory arthritis. *Rheumatology (Oxford)* 2019;58:e3-e42.
    PUBMED | **CROSSREF**

13. Park Y, Kwok SK. Recent advances in cell therapeutics for systemic autoimmune diseases. *Immune Netw* 2022;22:e10.
    PUBMED | **CROSSREF**

14. Wollin L, Wex E, Pautsch A, Schnapp G, Hostettler KE, Stowasser S, Kolb M. Mode of action of nintedanib in the treatment of idiopathic pulmonary fibrosis. *Eur Respir J* 2015;45:1434-1445.
    PUBMED | **CROSSREF**

15. Richeldi L, du Bois RM, Raghu G, Azuma A, Brown KK, Costabel U, Cottin V, Flaherty KR, Hansell DM, Inoue Y, et al. Efficacy and safety of nintedanib in idiopathic pulmonary fibrosis. *N Engl J Med* 2014;370:2071-2082.
    PUBMED | **CROSSREF**

16. King TE Jr, Bradford WZ, Castro-Bernardini S, Fagan EA, Glaspole I, Glassberg MK, Gorina E, Hopkins PM, Kardatzke D, Lancaster L, et al. A phase 3 trial of pirfenidone in patients with idiopathic pulmonary fibrosis. *N Engl J Med* 2014;370:2083-2092.
    PUBMED | **CROSSREF**

17. Aguilar S, Scotton CJ, McNulty K, Nye E, Stamp G, Laurent G, Bonnet D, Janes SM. Bone marrow stem cells expressing keratinocyte growth factor via an inducible lentivirus protects against bleomycin-induced pulmonary fibrosis. *PLoS One* 2009;4:e8013.
    PUBMED | **CROSSREF**

18. Ortiz LA, Gambelli F, McBride C, Gaupp D, Baddoo M, Kaminski N, Phinney DG. Mesenchymal stem cell engraftment in lung is enhanced in response to bleomycin exposure and ameliorates its fibrotic effects. *Proc Natl Acad Sci U S A* 2003;100:8407-8411.
    PUBMED | **CROSSREF**

19. Zhao F, Zhang YF, Liu YG, Zhou JJ, Li ZK, Wu CG, Qi HW. Therapeutic effects of bone marrow-derived mesenchymal stem cells engraftment on bleomycin-induced lung injury in rats. *Transplant Proc* 2008;40:1700-1705.
    PUBMED

20. Lee SH, Jang AS, Kim YE, Cha JY, Kim TH, Jung S, Park SK, Lee YK, Won JH, Kim YH, et al. Modulation of cytokine and nitric oxide by mesenchymal stem cell transfer in lung injury/fibrosis. *Respir Res* 2010;11:16.
    PUBMED | CROSSREF

21. Mahmoudi T, Abdolmohammadi K, Bashiri H, Mohammadi M, Rezaie MJ, Fathi F, Fakhari S, Rezaee MA, Jalili A, Rahmani MR, et al. Hydrogen peroxide preconditioning promotes protective effects of umbilical cord vein mesenchymal stem cells in experimental pulmonary fibrosis. *Adv Pharm Bull* 2020;10:72-80.
    PUBMED | CROSSREF

22. Liu M, Zeng X, Wang J, Fu Z, Wang J, Liu M, Ren D, Yu B, Zheng L, Hu X, et al. Immunomodulation by mesenchymal stem cells in treating human autoimmune disease-associated lung fibrosis. *Stem Cell Res Ther* 2016;7:63.
    PUBMED | CROSSREF

23. Zhao Y, Yan Z, Liu Y, Zhang Y, Shi J, Li J, Ji F. Effectivity of mesenchymal stem cells for bleomycin-induced pulmonary fibrosis: a systematic review and implication for clinical application. *Stem Cell Res Ther* 2021;12:470.
    PUBMED | CROSSREF

24. Li X, Yue S, Luo Z. Mesenchymal stem cells in idiopathic pulmonary fibrosis. *Oncotarget* 2017;8:102600-102616.
    PUBMED | CROSSREF

25. Hsu YC, Wu YT, Yu TH, Wei YH. Mitochondria in mesenchymal stem cell biology and cell therapy: from cellular differentiation to mitochondrial transfer. *Semin Cell Dev Biol* 2016;52:119-131.
    PUBMED | CROSSREF

26. Han S, Lee M, Shin Y, Giovanni R, Chakrabarty RP, Herrerias MM, Dada LA, Flozak AS, Reyfman PA, Khuder B, et al. Mitochondrial integrated stress response controls lung epithelial cell fate. *Nature* 2023;620:890-897.
    PUBMED | CROSSREF

27. Bernard O, Jeny F, Uzunhan Y, Dondi E, Terfous R, Label R, Sutton A, Larghero J, Vanneaux V, Nunes H, et al. Mesenchymal stem cells reduce hypoxia-induced apoptosis in alveolar epithelial cells by modulating HIF and ROS hypoxic signaling. *Am J Physiol Lung Cell Mol Physiol* 2018;314:L360-L371.
    PUBMED | CROSSREF

28. Islam MN, Das SR, Emin MT, Wei M, Sun L, Westphalen K, Rowlands DJ, Quadri SK, Bhattacharya S, Bhattacharya J. Mitochondrial transfer from bone-marrow-derived stromal cells to pulmonary alveoli protects against acute lung injury. *Nat Med* 2012;18:759-765.
    PUBMED | CROSSREF

29. Chambers DC, Enever D, Ilic N, Sparks L, Whitelaw K, Ayres J, Yerkovich ST, Khalil D, Atkinson KM, Hopkins PM. A phase 1b study of placenta-derived mesenchymal stromal cells in patients with idiopathic pulmonary fibrosis. *Respirology* 2014;19:1013-1018.
    PUBMED | CROSSREF

30. Glassberg MK, Minkiewicz J, Toonkel RL, Simonet ES, Rubio GA, DiFede D, Shafazand S, Khan A, Pujol MV, LaRussa VF, et al. Allogeneic human mesenchymal stem cells in patients with idiopathic pulmonary fibrosis via intravenous delivery (AETHER): a phase I safety clinical trial. *Chest* 2017;151:971-981.
    PUBMED | CROSSREF

31. Averyanov A, Koroleva I, Konoplyannikov M, Revkova V, Lesnyak V, Kalsin V, Danilevskaya O, Nikitin A, Sotnikova A, Kotova S, et al. First-in-human high-cumulative-dose stem cell therapy in idiopathic pulmonary fibrosis with rapid lung function decline. *Stem Cells Transl Med* 2020;9:6-16.
    PUBMED | CROSSREF

32. Sohni A, Verfaillie CM. Mesenchymal stem cells migration homing and tracking. *Stem Cells Int* 2013;2013:130763.
    PUBMED | CROSSREF

33. Ullah I, Subbarao RB, Rho GJ. Human mesenchymal stem cells - current trends and future prospective. *Biosci Rep* 2015;35:e00191.
    PUBMED | CROSSREF

34. Kretlow JD, Jin YQ, Liu W, Zhang WJ, Hong TH, Zhou G, Baggett LS, Mikos AG, Cao Y. Donor age and cell passage affects differentiation potential of murine bone marrow-derived stem cells. *BMC Cell Biol* 2008;9:60.
    PUBMED | CROSSREF

35. Zhang Y, Liao S, Yang M, Liang X, Poon MW, Wong CY, Wang J, Zhou Z, Cheong SK, Lee CN, et al. Improved cell survival and paracrine capacity of human embryonic stem cell-derived mesenchymal stem cells promote therapeutic potential for pulmonary arterial hypertension. *Cell Transplant* 2012;21:2225-2239.
    PUBMED | CROSSREF

36. Lian Q, Lye E, Suan Yeo K, Khia Way Tan E, Salto-Tellez M, Liu TM, Palanisamy N, El Oakley RM, Lee EH, Lim B, et al. Derivation of clinically compliant MSCs from CD105$^+$, CD24$^-$ differentiated human ESCs. *Stem Cells* 2007;25:425-436.
   PUBMED | CROSSREF

37. Karyana M, Djaharuddin I, Rif'ati L, Arif M, Choi MK, Angginy N, Yoon A, Han J, Josh F, Arlinda D, et al. Safety of DW-MSC infusion in patients with low clinical risk COVID-19 infection: a randomized, double-blind, placebo-controlled trial. *Stem Cell Res Ther* 2022;13:134.
   PUBMED | CROSSREF

38. Hübner RH, Gitter W, El Mokhtari NE, Mathiak M, Both M, Bolte H, Freitag-Wolf S, Bewig B. Standardized quantification of pulmonary fibrosis in histological samples. *Biotechniques* 2008;44:507-511.
   PUBMED | CROSSREF

39. Huang P, Zhou Y, Li XH, Zhang YN, Cheng HP, Fu JF, Liu W, Yue S, Luo ZQ. N-methyl-D-aspartate receptor blockers attenuate bleomycin-induced pulmonary fibrosis by inhibiting endogenous mesenchymal stem cells senescence. *Ann Transl Med* 2022;10:642.
   PUBMED | CROSSREF

40. Zhao X, Wu J, Yuan R, Li Y, Yang Q, Wu B, Zhai X, Wang J, Magalon J, Sabatier F, et al. Adipose-derived mesenchymal stem cell therapy for reverse bleomycin-induced experimental pulmonary fibrosis. *Sci Rep* 2023;13:13183.
   PUBMED | CROSSREF

41. Wu X, Gou H, Zhou O, Qiu H, Liu H, Fu Z, Chen L. Human umbilical cord mesenchymal stem cells combined with pirfenidone upregulates the expression of RGS2 in the pulmonary fibrosis in mice. *Respir Res* 2022;23:270.
   PUBMED | CROSSREF

42. Llontop P, Lopez-Fernandez D, Clavo B, Afonso Martín JL, Fiuza-Pérez MD, García Arranz M, Calatayud J, Molins López-Rodó L, Alshehri K, Ayub A, et al. Airway transplantation of adipose stem cells protects against bleomycin-induced pulmonary fibrosis. *J Investig Med* 2018;66:739-746.
   PUBMED | CROSSREF

43. Chen X, Wu Y, Wang Y, Chen L, Zheng W, Zhou S, Xu H, Li Y, Yuan L, Xiang C. Human menstrual blood-derived stem cells mitigate bleomycin-induced pulmonary fibrosis through anti-apoptosis and anti-inflammatory effects. *Stem Cell Res Ther* 2020;11:477.
   PUBMED | CROSSREF

44. Li X, Wang J, Cao J, Ma L, Xu J. Immunoregulation of bone marrow-derived mesenchymal stem cells on the chronic cigarette smoking-induced lung inflammation in rats. *BioMed Res Int* 2015;2015:932923.
   PUBMED | CROSSREF

45. Milosavljevic N, Gazdic M, Simovic Markovic B, Arsenijevic A, Nurkovic J, Dolicanin Z, Jovicic N, Jeftic I, Djonov V, Arsenijevic N, et al. Mesenchymal stem cells attenuate liver fibrosis by suppressing Th17 cells - an experimental study. *Transpl Int* 2018;31:102-115.
   PUBMED | CROSSREF

46. Kurihara K, Sasaki M, Nagahama H, Obara H, Fukushi R, Hirota R, Yoshimoto M, Teramoto A, Kocsis JD, Yamashita T, et al. Repeated intravenous infusion of mesenchymal stem cells enhances recovery of motor function in a rat model with chronic spinal cord injury. *Brain Res* 2023;1817:148484.
   PUBMED | CROSSREF

47. Takemura M, Sasaki M, Kataoka-Sasaki Y, Kiyose R, Nagahama H, Oka S, Ukai R, Yokoyama T, Kocsis JD, Ueba T, et al. Repeated intravenous infusion of mesenchymal stem cells for enhanced functional recovery in a rat model of chronic cerebral ischemia. *J Neurosurg* 2021;137:402-411.
   PUBMED | CROSSREF

48. Yang CC, Chen YL, Sung PH, Chiang JY, Chen CH, Li YC, Yip HK. Repeated administration of adipose-derived mesenchymal stem cells added on beneficial effects of empagliflozin on protecting renal function in diabetic kidney disease rat. *Biomed J* 2023:100613.
   PUBMED | CROSSREF

49. An L, Chu T, Wang L, An S, Li Y, Hao H, Zhang Z, Yue H. Frequent injections of high-dose human umbilical cord mesenchymal stem cells slightly aggravate arthritis and skeletal muscle cachexia in collagen-induced arthritic mice. *Exp Ther Med* 2021;22:1272.
   PUBMED | CROSSREF

50. Lee HJ, Lee WJ, Hwang SC, Choe Y, Kim S, Bok E, Lee S, Kim SJ, Kim HO, Ock SA, et al. Chronic inflammation-induced senescence impairs immunomodulatory properties of synovial fluid mesenchymal stem cells in rheumatoid arthritis. *Stem Cell Res Ther* 2021;12:502.
   PUBMED | CROSSREF